Self-Amplified HF Release and Polymer Deconstruction Cascades Triggered by Mechanical Force

Yixin Hu,[1] Liqi Wang,[1] Ilia Kevlishvili,[2] Shu Wang,[1] Chun-Yu Chiou,[1] Peyton Shieh,[3] Yangju Lin,[1,*] Heather J. Kulik,[2, 3,*] Jeremiah A. Johnson,[3,*] and Stephen L. Craig[1,*]

[1]Department of Chemistry, Duke University, Durham, North Carolina 27705, USA.

[2]Department of Chemical Engineering, Massachusetts Institute of Technology, Cambridge, MA 02139, USA.

[3]Department of Chemistry, Massachusetts Institute of Technology, Cambridge, MA 02139, USA.

KEYWORDS: Mechanochemistry, HF release, acid amplification, degradation.

ABSTRACT: Hydrogen fluoride (HF) is a versatile reagent for material transformation, with applications in self-immolative polymers, remodeled siloxanes, and degradable polymers. The responsive, *in situ* generation of HF in materials therefore holds promise for new classes of adaptive material systems. Here, we report the mechanochemically coupled generation of HF from alkoxy-*gem*-difluorocyclopropane (*g*DFC) mechanophores derived from difluorocarbene addition to enol ethers. Production of HF involves an initial mechanochemically assisted rearrangement of *g*DFC mechanophore to α-fluoro allyl ether whose regiochemistry involves preferential migration of fluoride to the alkoxy substituted carbon, and ab initio steered molecular dynamics simulations reproduce the observed selectivity and offer insights into the mechanism. When the alkoxy *g*DFC mechanophore is derived from poly(dihydrofuran), the α-fluoro allyl ether undergoes subsequent hydrolysis to generate one equivalent of HF and cleave the polymer chain. The hydrolysis is accelerated via acid catalysis, leading to self-amplifying HF generation and concomitant polymer degradation. The mechanically generated HF can be used in combination with fluoride indicators to generate optical response and to degrade poly(norbornene) with embedded HF-cleavable silyl ethers (20 mol%). The alkoxy-*g*DFC mechanophore thus provides a mechanically coupled mechanism of releasing HF for polymer remodeling pathways that complements previous thermally driven mechanisms.

INTRODUCTION

Mechanochemistry has been widely applied in various contexts, including mechanochromic materials,[1-3] mechanocatalysis,[4, 5] unlocking otherwise inaccessible reactions,[6-10] small molecule release,[11-15] and to enhance the mechanical properties of networks integrated with mechanophores.[16, 17] Among these applications, the mechanically triggered release of acid is useful for a rich range of responses, including acid-induced polymer degradation,[18-20] polymerization,[21] and hydrogel actuators.[22-25] The concept of a mechanochemically generated acid was first reported by Diesendruck *et al.* using a *gem*-dichlorocyclopropanated (*g*DCC) indene (Figure 1),[12] which was followed by a more thermally stable, but scissile, design based on an oxime sulfonate mechanophore.[26] More recently, some of us reported easily synthesized alkoxy-substituted *g*DCC mechanophores that readily releases hydrochloric acid in a non-scissile fashion similar to the indene, but with improved thermal stability – combining some of the more attractive attributes of previous designs.[27, 28]

Inspired by the prior success with mechanically driven HCl release, we wondered about the potential to develop a system that can mechanically release hydrogen fluoride (HF), an important multipurpose reagent for both laboratory and industrial applications. Much of the chemistry of HF is unique relative to HCl and other common acids. While HF is widely used in the synthesis of fluorine-containing compounds, such as fluoropolymers[29] and pharmaceutical intermediates,[30] we were drawn to its use as a versatile reagent for material remodeling. In particular, fluoride sources react readily with silica-containing materials, and this efficient characteristic has been applied in self-immolative polymers,[31] remodeled siloxane elastomers,[32, 33] vitrimer alteration,[34] and degradable polymers.[18, 35, 36] The corrosiveness and toxicity of HF,[37] however, presents a safety concern for its handling and storage.[38] We therefore set out to develop a latent source of HF that resides within a polymer until released in response to a mechanical signal, at which point it could be converted in situ to a fluoride salt for the uses described above.

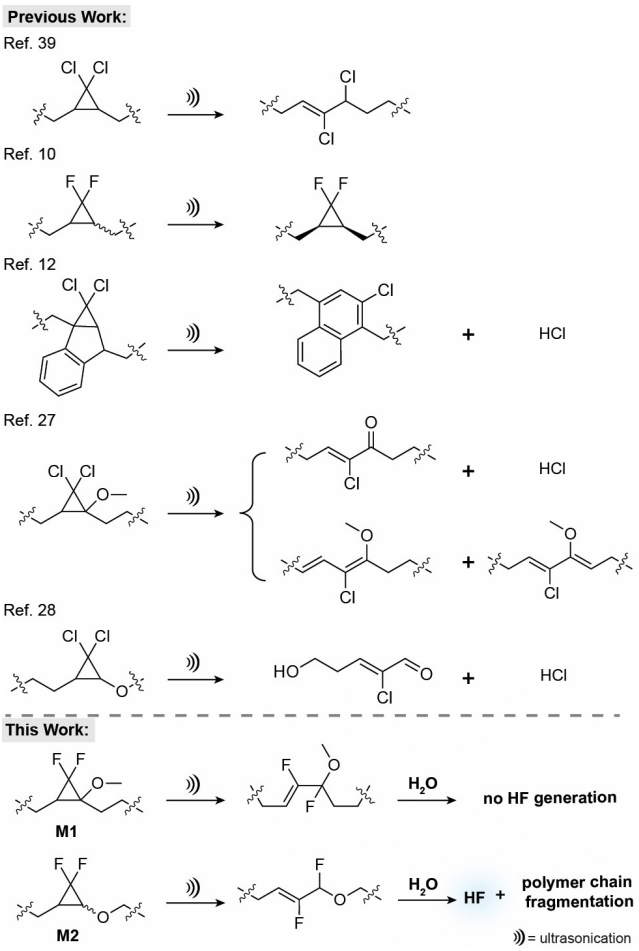

Figure 1. Schematic representation of previously reported mechanophores[10, 12, 27, 28, 39] and the mechanical release of hydrogen fluoride reported in this work.

In designing a mechanophore for fluoride release, we considered that the addition of a methoxy substituent to a *gem*-dichlorocyclopropane (*g*DCC) mechanophore yielded a 2-methoxy-substituted *gem*-dichlorocyclopropane (MeO-*g*DCC)[27] that acts as a latent source of HCl (Figure 1). Despite the similarities in HF and HCl, we anticipated that a 2-methoxy-*gem*-difluorocyclopropane (MeO-*g*DFC) mechanophore would be a far less effective (and perhaps entirely ineffective) source of mechanically generated HF than its chlorinated analog. We perceived two potential primary barriers. First, the ring-opening reaction of the parent dialkyl *g*DFC[10] differs from that of *g*DCC. The ring opening of *g*DCC involves presumably concerted C-C bond scission and chloride migration, leading to the formation of an α-chloro allyl ether product. In contrast, *g*DFC ring opening in the parent system (either thermal or mechanical) involves a 1,3-diradicaloid transition state (thermal) or force-coupled intermediate (mechanical) that recloses back to the original *g*DFC structure or its stereoisomer; dissociation/migration of fluoride is not observed.[7, 10] Second, even if the corresponding α-fluoro allyl ether were generated (in part or in whole), the elimination of HF is generally disfavored relative to that of HCl. For example, in the aromatization of 1,1-dihalo-6,6a-dihydro-1aH-cyclopropa[a]indene through HX elimination, HF elimination requires temperatures of 160 °C[40] to achieve rates comparable to those achieved for HCl elimination at 50 °C.[12] Nonetheless, we began our pursuit of HF generating mechanophores by exploring the mechanochemistry of two polymers that incorporate alkoxy-substituted *g*DFCs along their backbones (Figure 1): **P1** – a copolymer of MeO-*g*DFC that is analogous to the previously reported MeO-*g*DCC mechanoacid, and **P2** – the polymer generated from exhaustive difluorocarbene addition to poly(dihydrofuran) (PDHF).

Here we report a range of outcomes initiated by the mechanochemical reactivity of these polymers, as induced by pulsed sonication of their solutions. First, the addition of the alkoxy substituent leads to irreversible ring opening and regiospecific fluoride migration to yield the corresponding α-fluoro allyl ether product. Second, the presence of water enables the hydrolysis of ring opened **P2** in a reaction sequence that also generates HF. Third, the aforementioned hydrolysis is accelerated by HF, leading to self-amplifying HF production and polymer deconstruction. Finally, the fluoride generated can be used to generate optical signals in the presence of suitable fluoride sensors, or as the transduction agent within a polymer degradation cascade that couples HF generation to the cleavage of silyl ether linkers.[18, 35, 41, 42]

RESULTS AND DISCUSSION

Synthesis and characterization. As shown in Scheme 1, we synthesized the MeO-*g*DFC macrocycle **4** from the selective difluorocyclopropanation of commercially available 1-methoxy-1,4-cyclohexadiene at the electron-rich alkene position, followed by subsequent ozonolysis, esterification, and ring-closing metathesis (RCM). A copolymer **P1** of 9-oxabicyclo[6.1.0]non-4-ene (epoxy-COD) and **4** was obtained through ring-opening metathesis polymerization (ROMP),[43] as employed previously for the synthesis of multi-mechanophore polymers.[10, 27] The related polymer **P2** was synthesized through difluorocyclopropanation of PDHF using $TMSCF_3$ and NaI at 100 °C in a pressurized vessel under N_2.[44] The isolated **P1** and **P2** contain alkoxy *g*DFC mechanophores **M1** and **M2** (Table 1), respectively, and their mechanochemistry was investigated using sonication, under which conditions the epoxy unit in **P1** has been found to be mechanically inactive.[6, 7, 13, 45] The different synthetic pathways lead to polymers of differing number-averaged molar mass (M_n), but, as discussed below, M_n does not influence the product generated by the mechanochemically induced chemistry.

Scheme 1. Synthesis of (a) P1 and (b) P2.

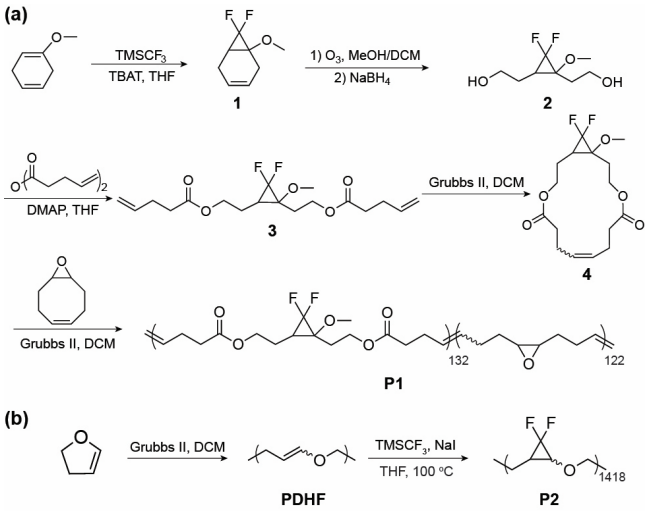

Table 1. Characterization of **P1** and **P2**.

	M_n (kDa)	$Đ$	**M1**%	**M2**%	#**M1**	#epox	#**M2**
P1	59	1.8	52	-	132	122	-
P2	210	1.6	-	100	-	-	1418

Molar masses (M_n) and dispersity ($Đ$) determined by size exclusion chromatography and multi-angle light scattering. Fractional content of **M1** or **M2** repeats determined by 1H NMR, and average number of **M1**, **M2**, or epoxide (epox) repeats per polymer by combining the two measurements.

Mechanically triggered fluoride migration. **P1** and **P2** were dissolved in 11 mL of dry tetrahydrofuran (THF) at a concentration of 2 mg/mL. The resulting solutions were subjected to ultrasonication for 4

h (1s on and 1s off, 30% amplitude, 4-9 °C in N_2), and the products were analyzed by nuclear magnetic resonance (NMR) and size exclusion chromatography (SEC). As is characteristic of polymer mechanochemistry in multi-mechanophore polymers, a concomitant reduction in number-average molar mass (M_n, from 59 to 24 kDa) and mechanophore activation (up to 80%) is observed in **P1** with ongoing sonication, tapering as M_n approaches an apparent so-called limiting M_n (Figure 2a). The reduction in M_n during sonication is attributed to random scission of bonds along the backbone, which occurs even though the mechanophores non-scissile.[27, 46] Whereas dialkyl *g*DFC mechanophores undergo predominant ring-opening/ring-closing and *trans*/*cis* isomerization,[6, 8, 10] sonication of **P1** results in a new set of resonances in the ^{19}F NMR spectrum that are consistent with the conversion of **M1** into the ring-opened α-fluoro allyl ether product **A1** (Figure 2b). The ^{19}F NMR spectrum of **A1** has two peaks that integrate in a 1:1 ratio – a triplet (J = 17.3 Hz) at –123.6 ppm and a doublet (J = 36.6 Hz) at –125.5 ppm that are consistent with assignments to $\mathbf{F_B}$ and $\mathbf{F_A}$ respectively (Figure 2c). The ^{1}H NMR also shows a doublet of triplets at 5.3 ppm and a new singlet at 3.3 ppm which match the vinyl proton and methoxy protons of **A1**, respectively (Figure S3).

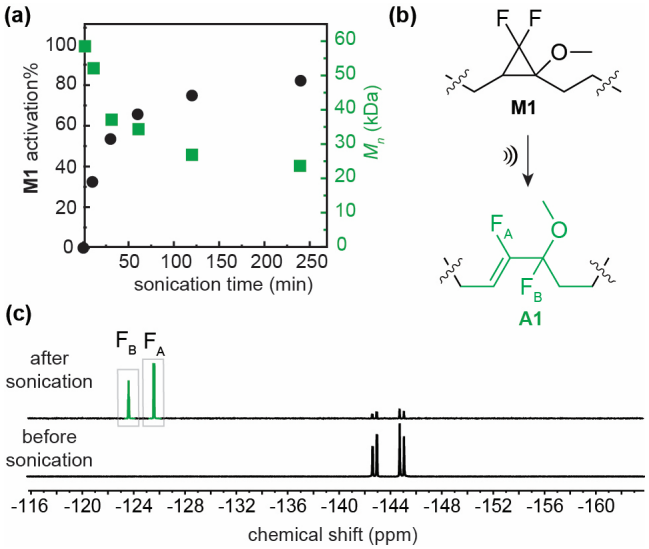

Figure 2. (a) Conversion of **M1** (black circles) and M_n of **P1** (green squares) as a function of sonication time; (b) Mechanochemical reaction of **M1** induced by sonication; (c) ^{19}F NMR spectrum of **P1** in THF-d_8 before and after 4 h sonication.

The clean isomerization of **M1** to **A1** is distinct from the reactivity of its MeO-*g*DCC analog, which results in a mixture of products that involve net elimination of either HCl or MeCl. Insights into the unique reactivity of **M1** are gleaned from DFT calculations. Ab initio steered molecular dynamics (AISMD) simulations were performed for the MeO-*g*DFC and MeO-*g*DCC mechanophores. Propyl groups were used as surrogates of the polymer attachments. A force of 2 nN was applied to the terminal carbon atoms of the propyl handles. In the simulations, the MeO-*g*DCC ring undergoes dynamically concerted ring cleavage accompanied by chloride dissociation, which generates an allylic carbocation intermediate (Figure 3a). Inspection of the $\langle S^2 \rangle$ values (i.e., the expectation value of the S^2 operator) during the MD simulation shows that this process is heterolytic, with the value of $\langle S^2 \rangle$ never rising above 0.25 (Figure 3a, Table S5). This observation suggests that there is no diradical character formed during the ring-opening step (Figure 3a, Table S4). This intermediate is primed to undergo either deprotonation to generate HCl or S_N2 substitution at the methyloxonium to generate MeCl. In contrast, **M1** ring opening occurs through initial homolytic cleavage of the C-C bond. The diradical intermediate is dynamically stable and long lived under the external force of 2 nN (Figure 3b). Furthermore, the diradical intermediate undergoes fluorine atom transfer coupled with an electron transfer, as seen from a sharp decline in $\langle S^2 \rangle$ value coupled with C–F bond elongation, leading to fluoride anion dissociation and a rebound to the carbon center (Figure 3b). In these simulations, the charge-separated complex is very short-lived likely due to the absence of explicit treatment of solvent (Figure 3b). While both fluoride migration regioisomers were observed during molecular dynamics simulations, the predominant pathway was migration to the methoxy substituted carbon (Table S5). Despite discrepancies in experimentally observed regioselectivity, which can be attributed to the lack of explicit treatment of solvent, computational results can rationalize the regioselectivity of the migration observed experimentally. The methoxy-substituted carbon has a higher charge throughout MD trajectories, and the recombined product is thermodynamically favorable by 12.3 kcal/mol (Table S5, Figure S36).

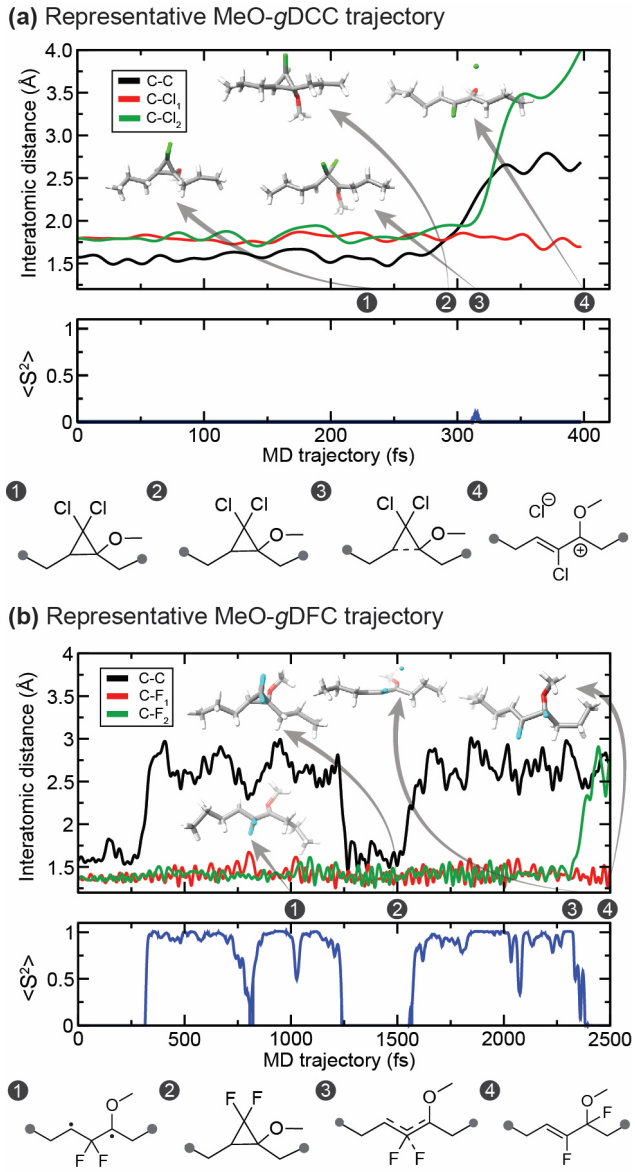

Figure 3. Representative molecular dynamics simulation trajectories with MeO-*g*DFC (a) and MeO-*g*DCC (b) mechanophores. Cleaving C-C distance and two C-X distance plots are shown at the top and $\langle S^2 \rangle$ values are shown in the bottom. Structures along the trajectory are shown as insets (C in gray, H in white, O in red, Cl in green, F in cyan). Associated chemical structures are provided below each MD trajectory.

Similar regioselectivity is observed in the sonication behavior of poly(alkoxy-*g*DFC) **P2** derived from PDHF (Figure 4). Like **P1**, when **P2** is sonicated in THF over 4 h, there is a decrease from initial M_n of 210 kDa to a gradually tapering value of 43 kDa. At the same time, ^{19}F and ^{1}H NMR indicate that embedded **M2** is mechanically active and

rearranges in a manner that is analogous to **M1**. **M2** exists as two stereoisomers: a *cis* isomer that corresponds to the ^{19}F NMR peaks at δ = -129.3 and -158.9 ppm, and a *trans* isomer with peaks at δ = -140.9 and -144.3 ppm. The isomers produce the same product but have different reactivities under sonication; the more mechanochemically reactive *cis* isomer is converted more quickly during sonication (see Table S1). Fluorine atom migration to yield product **A2** is inferred from the appearance of two new signals $\mathbf{F_C}$ and $\mathbf{F_D}$ that integrate 1:1—a doublet of doublets at –129.8 ppm (J = 62.6, 19.4 Hz) and a doublet of doublets of doublets at –129.4 ppm (J = 37.5, 19.4, 8.2 Hz), respectively. In the ^{1}H NMR spectrum, a new doublet of triplets at 5.2 ppm is assigned to the vinyl proton on **A2** (Figure S8). Figure 4 shows that the product of the reaction stays the same with continuing sonication across multiple scissions per polymer chain; in other words, the product of the mechanochemical reaction does not change with polymer M_n, as mentioned above. As with **M1**, the presence of the alkoxy substituent directs a highly regioselective migration of fluorine to generate the α-fluoro allyl ether product.

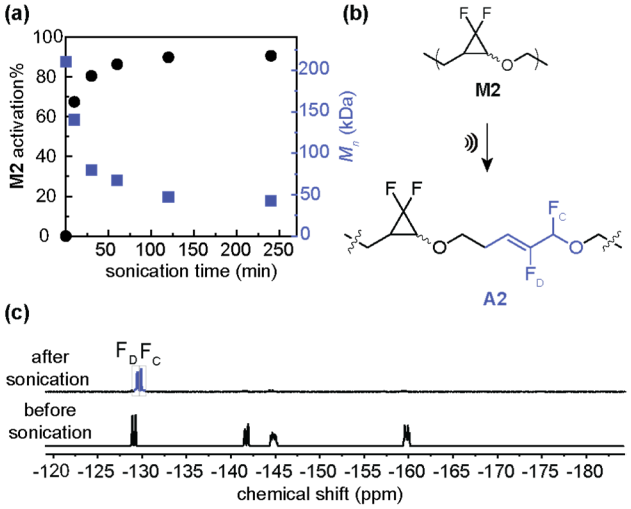

Figure 4. (a) Conversion of **M2** (black circles) and M_n of **P2** (blue squares) as a function of sonication time; (b) Mechanochemical reaction of **M2** induced by sonication; (c) ^{19}F NMR spectrum of **P2** in THF-d_8 before and after 4 h sonication.

Hydrolytic HF generation and chain scission. The sonication behavior of **P2** changes when 10% (v/v) water is added to the THF, whereas **P1** remains unaffected. After only 10 min sonication, the M_n of **P2** drops to 47 kDa, as opposed to 140 kDa in the absence of water. The increase in the initial rate of M_n reduction is accompanied by a greater extent to which M_n ultimately changes. After 4 h sonication, the M_n with water present is 10 kDa, in comparison to an apparently limiting value of 43 kDa without water added (Figure 5a). Interestingly, the extent of **M2** activation is not significantly changed by the presence of water (Figures 5a, S16-17); only the ultimate product of activation differs. As described below, the change in product is a consequence of reactivity that occurs after, rather than during, mechanochemical conversion of **M2** to **A2**.

The reactivity of **A2** with water was probed by first sonicating **P2** in THF-d_8 and then adding 100 μL water to 0.9 mL of the post-sonicated solution. The results are consistent with the hydrolytic conversion of allyl ether **A2** into lower molecular species **A3** and **A4** (Figure 5b). Over the course of 33 h at room temperature, the ^{19}F NMR resonances from $\mathbf{F_C}$ and $\mathbf{F_D}$ disappear and a new doublet of doublets (J = 33.3, 19.1 Hz) emerges at –135.4 ppm (Figure 5c). The chemical shift and splitting pattern are consistent with the assignment of vinyl fluorine $\mathbf{F_E}$ on the backbone. This assignment is further supported by the observation that ^{1}H NMR peaks at 9.2 ppm and 6.3 ppm (the aldehyde proton and vinyl proton in **A3**, respectively) are coupled to the $\mathbf{F_E}$ resonance (Figure S14). Furthermore, gas chromatography–mass spectrometry of the reaction solution gives M_n matching those of **A3** and small **A4** oligomers (Table S2). Finally, the production of **A3** and **A4** implies the generation of HF as a hydrolysis by-product, and two new ^{19}F NMR resonances at –152.1 and –180.1 ppm match the chemical shifts observed when aqueous HF (48% in H_2O) is added to THF-d_8 (Figure S16). **Note: the use and/or generation of HF requires proper attention to safety protocols**; see Supplementary Information for details.

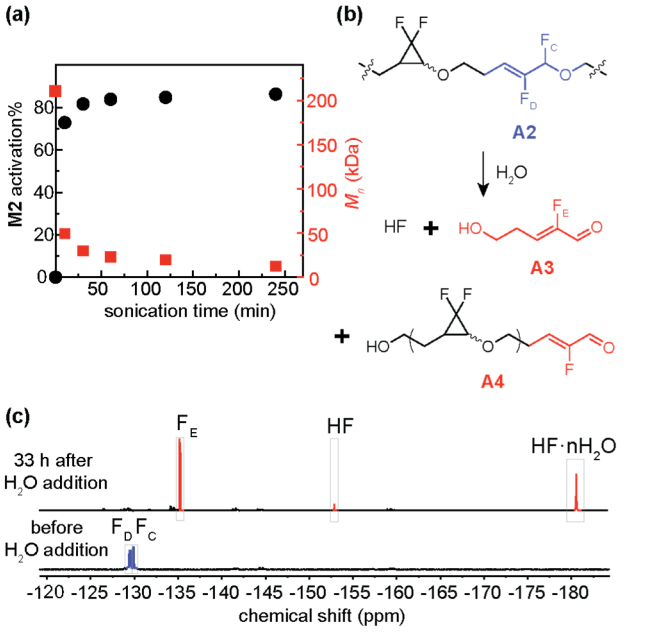

Figure 5. (a) Activation of **P2** (black circles) during sonication with H_2O and M_n of **P2** (red squares) as a function of sonication time; (b) Proposed final products of **A2** after ring opening and reaction with H_2O; (c) Spectrum of ^{19}F NMR in THF-d_8 before and after H_2O addition.

Autocatalysis and amplification. The time course of the hydrolysis reveals unexpected kinetic complexity in the conversion of **A2** into the products shown above. In a separate experiment, 100 μL H_2O was added to 0.9 mL of a dry THF solution of **P2** that had been sonicated for 4 h. The progress of the reaction at room temperature was followed by ^{19}F NMR. As seen in Figure 6a, the initial rate of hydrolysis is very slow, with only a few percent conversion observed over the first 10 h. Soon after, the rate increases and conversion completes within 33 h. The gradual increase in rate of reaction suggests an autocatalytic effect of the products, most likely as a result of the generated HF. To probe that hypothesis, 5 μL of aqueous HF (48% in H_2O) was added with water to the freshly sonicated **P2**. The additional HF corresponds to 7.3 times that produced by the complete conversion of **M2**. Conversion of **A2** occurs much more rapidly, going to completion in less than 30 min vs. over 20 h without added HF. The reaction catalysis is attributed to the acidic character of HF, rather than the presence of fluoride. Addition of CF_3COOH also accelerates the hydrolysis, whereas addition of tetrabutylammonium fluoride does not (Figures S24 & S25). One potential mechanism that is consistent with the experimental observations involves acid-catalyzed ether hydrolysis through nucleophilic displacement, followed by elimination of HF from the resulting fluorohydrin (Scheme S1).

The conversion of **A2** in the post-sonication hydrolysis is accompanied by a further reduction in polymer M_n, consistent with a reaction that includes chain scission (Figure 6b). The observed reduction in M_n can be quantitatively attributed to the hydrolysis. If one assumes that the reduction in M_n is due entirely to a hydrolysis reaction that generates HF, then the relationship between degree of polymerization and conversion of α-fluoro allyl ether is given by equation (1) (see S18 for detailed derivation), below:

$$\frac{1}{DP(c)} = c + \frac{1}{DP_0} \qquad (1)$$

Here, DP is the degree of polymerization of **P2** given by $DP = M_n/120$, where M_n is the number-averaged molar mass determined by size-exclusion chromatography and multi-angle light scattering (SEC-MALS), and 120 is the mass of the repeat unit; c is the fractional conversion of α-fluoro allyl ether, given by ([HF]+[**A3**]+[**A4**])/([HF]+[**A2**]+[**A3**]+[**A4**]) and obtained by ^{19}F NMR; and DP_0 is the initial degree of polymerization. As seen in Figure 6c, a plot of 1/DP vs. c at low conversion agrees well with eq. 1. At higher conversion, the apparent M_n is overestimated (and 1/DP is underestimated) due to the increasing presence of low-molar mass degradation products that are not included in the SEC-MALS analysis, which precludes a quantitative evaluation of the relationship between hydrolysis and chemical scission across the entire degradation time.

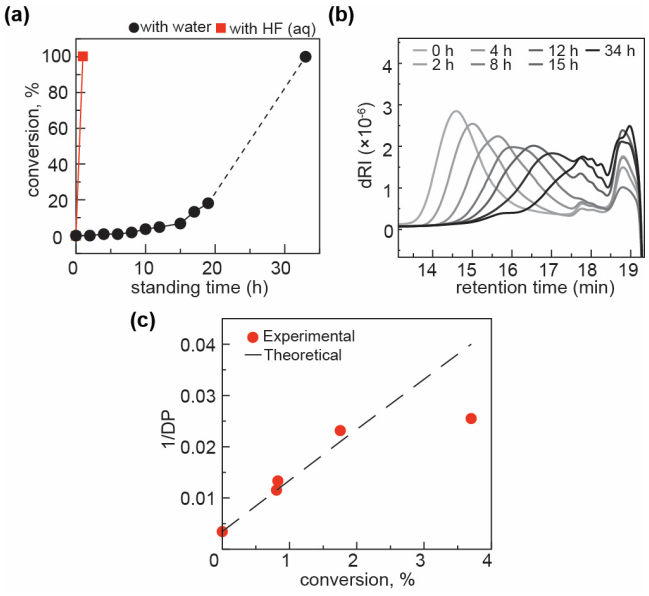

Figure 6. (a) Conversion vs. post-sonication standing time of **A2** with 10% (v/v) addition of H_2O (black circles) and 10% (v/v) addition of H_2O and 5 μL HF (red squares) at room temperature. Lines provided to guide the eye. (b) SEC chromatograms of post-sonicated **A2** as a function of time following addition of 10% (v/v) H_2O. (c) Experimental 1/DP vs. conversion at different standing times following addition of 10% (v/v) H_2O. The line is the theoretical expectation (eq. 1).

The hydrolysis reaction appears to be dominated by the reactivity of the α-fluoro allyl ether product of sonication, rather than by reaction of water with, for example, a tension trapped oxonium intermediate during the sonication-induced chain extension. We compared the extent of HF generation and M_n of **P2** that was sonicated for 4 h in the presence of water to **P2** that was sonicated for 4 h in the absence of water and then allowed to react with water for an additional 4 h. Both the amount of HF (0.9% and 0.8%, respectively) and molar mass (12.3 kDa and 10.1 kDa, respectively) are quite similar for the two experiments (Figure S16). We cannot rule out that some direct hydrolysis takes place during the mechanochemical events triggered in the presence of water. Given the autocatalytic effect of HF generation, however, any such events must be rare for the two experiments to generate such similar results.

Applications of released HF. The reactivity of the HF released by the cascading hydrolysis can be used to generate additional outcomes in the presence of the other products of **P2** degradation. For example, optical signals can be induced in the presence of base and the pro-fluorescent fluoride indicator tert-butyldiphenylsilyl-protected 7-hydroxy-4-tri-fluoromethylcoumarin (TBDPSCA, **probe 5**).[47] To minimize water content, only 10 μL of H_2O was added to 1 mL of post-sonicated **P2**. After the conversion of **P2** was completed, 10 μL *N,N*-diisopropylethylamine (DIPEA) was added to deprotonate the HF. Finally, 10 μL of **probe 5** was added to the solution. When irradiated at 365 nm, the solution emits the expected blue-green color associated with the deprotected coumarin. In contrast, the same operation applied to **P1** leads to no discernable visible fluorescence by eye (Figure 7b) or via spectroscopy (Figure 7c). For comparison, the absence of DIPEA in the mixture of **P2** and water resulted in a lack of observable fluorescence (Figure S26). This indicates the crucial role of ionizing HF in producing a distinct fluorescence color.

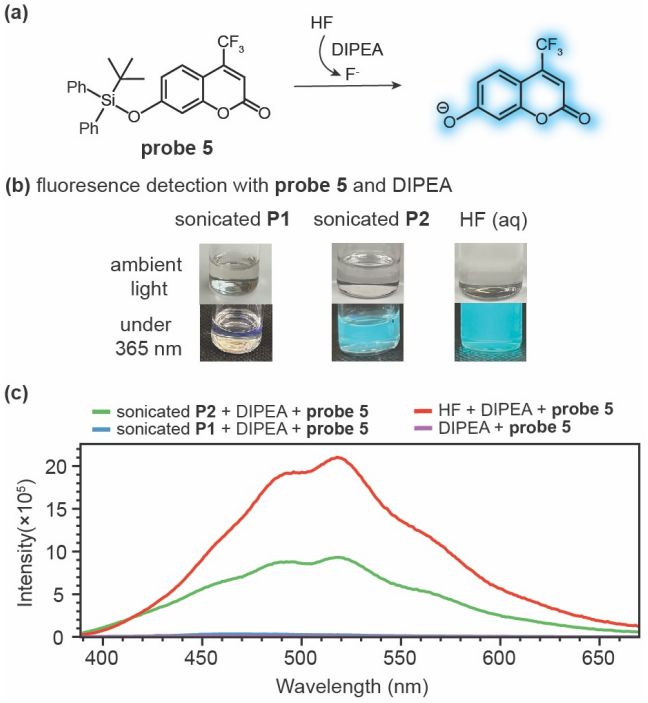

Figure 7. (a) Working scheme of fluoride ion detector probe; (b) Detection of fluoride by adding **probe 5** and DIPEA to post sonicated **P1**, post sonicated **P2** and the control group of HF (48% in H_2O); (c) fluorescence spectra of experimental groups (sonicated **P1** and **P2**) and control groups (HF (aq)+DIPEA+ **probe 5**, DIPEA + **probe 5**; all control groups are with same concentration of DIPEA and **probe 5**).

We speculated that it could be possible to combine the HF generation available in **P2** with polymers possessing HF-sensitive motifs, enabling the stress-triggered degradation of a wider range of material systems. This concept requires a delicate balance of kinetic considerations: the reactivity of the degradable unit to HF should be slow relative to the self-amplifying chemistry, else the degradation reaction would effectively quench the amplification and limit the ultimate extent of degradation. We chose for this purpose a diisopropyl silyl ether, which is labile upon exposure to HF.[18, 35] The polymer **P3** was synthesized with 11% of the repeats along its polybutadiene backbone containing the desired silyl ether, which has been recently applied in degradable polymers that are selectively cleaved by fluoride.[31] The polybutadiene control **P4**, without a silyl ether, was also synthesized (Figure 8a).

Two initial control experiments aimed to assess the stability of post-sonicated **P4** in the presence of mechanochemically generated HF and water, as well as the stability of post-sonicated **P3** with water but without the HF source. A mixture of **P4** and **P2** (each at 2 mg/mL) was sonicated in THF:H_2O (95/5, v/v) for 4 h. Analysis of the polybutadiene component **P4** in the post-sonicated solution is facilitated by the drastic degradation and reduction in M_n of **P2** described above, which as expected leads **P2** to disappear from the 13.5-16.5 min retention time window over the first 2 days following sonication. The degradation of **P2** alone with 5% (v/v) H_2O in THF, characterized SI, is evident in Figure 8b through the change in shape of the SEC elugram at 2 d relative to its appearance immediately following sonication. The peak is broader immediately following sonication (red trace, Figure 8b) and narrows over 2 d due to a reduction in the higher retention time/lower M_n side of the

peak (grey trace). From ^{19}F NMR (Figure S28), **P2** gradually decomposed to HF and other final products throughout 4 days. As seen in Figure 8b, a significant fraction of the peak in the 13.5-16.5 min retention time window remains stable for up to 14 days post-sonication, and we assign this peak to **P4**. The assignment of **P4** is supported by the fact that the retention times and M_n observed match those of **P4** sonicated without **P2** (Figure 8c). The key point is that while sonication initially cleaves **P4** through unspecific mechanochemical bond scission, the M_n of post-sonicated **P4** (in contrast to **P2**) does not change upon standing for up to 14 d. Similar behavior is seen when **P3**, which contains the silyl ether, is sonicated for 4 h in the absence of **P2** (Figure 8d). Thus, the polybutadiene backbone is not reactive to the products of sonicated **P2**, and the silyl ether in **P3** is stable post-sonication in the absence of **P2**.

The combination of **P2** and **P3**, however, results in the desired two-stage response to sonication, as seen in Figure 8e. First, the degradation of **P2**, and the associated HF generation, over the first two days post-sonication is still evident (red vs grey traces, Figure 8e). The expected reactivity is confirmed by ^{19}F NMR (Figure S28). Thus, the presence of the silyl ether in **P3** does not appear to substantially affect the **P2** self-amplifying behavior. Second, from day 2 to day 14, the targeted deconstruction of **P3** is observed, as evidenced by increasing retention times in the SEC traces. Because this second effect is not observed in controls when either the silyl ether or the HF source is absent, we attribute the overall behavior to mechanochemical activation of **P2** initiating the (relatively rapid) self-amplifying release of HF via acid-catalyzed main-chain hydrolysis, followed by the (relatively slow) HF-induced breaking of the silyl ether Si-O bond.

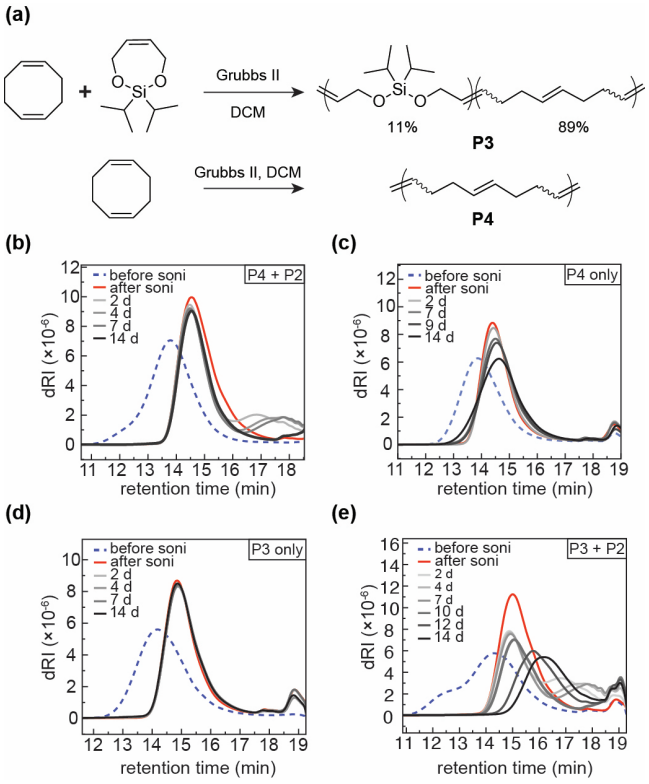

Figure 8. (a) Silyl ether copolymers **P3** for degradation and control group of **P4**; SEC traces of (b) **P4** + **P2**, (c) **P4**, (d) **P3**, (e) **P3** + **P2** before (blue dashed line) and after (red solid line) 4 h sonication with 95:5 THF:H_2O. At 2-14 days of standing time following sonication, any **P2** component has degraded to the point that the remaining SEC traces reflect changes in the M_n of **P3** or **P4** (grey to black solid lines).

CONCLUSIONS

The addition of alkoxy substituents to *gem*-difluorocyclopropane mechanophores induces a combination of reactivity outcomes that differ from prior unsubstituted *g*DFC. Whereas unsubstituted *g*DFC reversibly opens to give tension-trapped diradical species, **P1** and **P2** irreversibly open with associated fluorine migration. AISMD simulations suggest a mechanism that involves a mixture of homolytic bond scission, fluorine atom dissociation, electron transfer, and anion rebound, ultimately leading to regioselective fluorine migration and the formation of the observed product. A reduced number of carbon substituents at the secondary carbon of the cyclopropane ring, as in **P2**, opens the door for the subsequent release of HF in an autocatalytic fashion. The HF is generated through a hydrolysis reaction that also leads to chain scission, and the resulting amplified degradation provides a tool that complements recent approaches to self-immolative polymers.[48-51] The amplified production of HF can also be harvested for triggered degradation of a separate set of polymer linkages formed via diisopropyl silyl ethers, whose reaction with HF is slower than the autocatalytic reaction. This efficient and controllable HF release capability could have significant implications for the future applications of HF in responsive disassembly and remodeling of polymer networks based on fluoride-sensitive junctions.

ASSOCIATED CONTENT

Supporting Information

The Supporting Information is available free of charge on the ACS Publications website.

Synthetic procedures and characterizations. Computational details. (PDF)

AUTHOR INFORMATION

Corresponding Author

*stephen.craig@duke.edu
*kulik@mit.edu
*jaj2109@mit.edu

Author Contributions

The manuscript was written through contributions of all authors. / All authors have given approval to the final version of the manuscript.

Funding Sources

This work was supported by the NSF Center for the Chemistry of Molecularly Optimized Networks (MONET; Award CHE-2116298) and Duke University.

ACKNOWLEDGMENT

This work was supported by the NSF Center for the Chemistry of Molecularly Optimized Networks (MONET; Award CHE-2116298) and Duke University.

ABBREVIATIONS

*g*DFC, *gem*-difluorocyclopropane; *g*DCC, *gem*-dichlorocyclopropane; DIPEA, *N,N*-diisopropylethylamine; SEC, size exclusion chromatography; M_n, number-averaged molar mass; THF, tetrahydrofuran; PDHF, polydihydrofuran

REFERENCES

(1) Davis, D. A.; Hamilton, A.; Yang, J.; Cremar, L. D.; Van Gough, D.; Potisek, S. L.; Ong, M. T.; Braun, P. V.; Martinez, T. J.; White, S. R.; et al. Force-Induced Activation of Covalent Bonds in Mechanoresponsive Polymeric Materials. *Nature* **2009**, *459* (7243), 68-72. DOI: 10.1038/nature07970.

(2) Zhang, H.; Gao, F.; Cao, X.; Li, Y.; Xu, Y.; Weng, W.; Boulatov, R. Mechanochromism and Mechanical-Force-Triggered Cross-Linking from a Single Reactive Moiety Incorporated into Polymer Chains. *Angew. Chem. Int. Ed.* **2016**, *55* (9), 3040-3044. DOI: 10.1002/anie.201510171.

(3) Imato, K.; Kanehara, T.; Ohishi, T.; Nishihara, M.; Yajima, H.; Ito, M.; Takahara, A.; Otsuka, H. Mechanochromic Dynamic Covalent Elastomers: Quantitative Stress Evaluation and Autonomous Recovery. *ACS Macro Lett.* **2015**, *4* (11), 1307-1311. DOI: 10.1021/acsmacrolett.5b00717.

(4) Piermattei, A.; Karthikeyan, S.; Sijbesma, R. P. Activating Catalysts with Mechanical Force. *Nat. Chem.* **2009**, *1* (2), 133-137. DOI: 10.1038/nchem.167.

(5) Kean, Z. S.; Akbulatov, S.; Tian, Y.; Widenhoefer, R. A.; Boulatov, R.; Craig, S. L. Photomechanical Actuation of Ligand Geometry in Enantioselective Catalysis. *Angew. Chem.* **2014**, *53* (52), 14508-14511. DOI: 10.1002/anie.201407494.

(6) Wang, J.; Kouznetsova, T. B.; Craig, S. L. Single-Molecule Observation of a Mechanically Activated Cis-to-Trans Cyclopropane Isomerization. *J. Am. Chem. Soc.* **2016**, *138* (33), 10410-10412. DOI: 10.1021/jacs.6b06452.

(7) Wang, J.; Kouznetsova, T. B.; Niu, Z.; Ong, M. T.; Klukovich, H. M.; Rheingold, A. L.; Martinez, T. J.; Craig, S. L. Inducing and Quantifying Forbidden Reactivity with Single-Molecule Polymer Mechanochemistry. *Nat. Chem.* **2015**, *7* (4), 323-327. DOI: 10.1038/nchem.2185.

(8) Wang, J.; Ong, M. T.; Kouznetsova, T. B.; Lenhardt, J. M.; Martinez, T. J.; Craig, S. L. Catch and Release: Orbital Symmetry Guided Reaction Dynamics from a Freed "Tension Trapped Transition State". *J. Org. Chem.* **2015**, *80* (23), 11773-11778. DOI: 10.1021/acs.joc.5b01493.

(9) Wang, J.; Kouznetsova, T. B.; Craig, S. L. Reactivity and Mechanism of a Mechanically Activated Anti-Woodward-Hoffmann-Depuy Reaction. *J. Am. Chem. Soc.* **2015**, *137* (36), 11554-11557. DOI: 10.1021/jacs.5b06168.

(10) Lenhardt, J. M.; Ong, M. T.; Choe, R.; Evenhuis, C. R.; Martinez, T. J.; Craig, S. L. Trapping a Diradical Transition State by Mechanochemical Polymer Extension. *Science* **2010**, *329* (5995), 1057-1060. DOI: 10.1126/science.1193412.

(11) Larsen, M. B.; Boydston, A. J. "Flex-Activated" Mechanophores: Using Polymer Mechanochemistry to Direct Bond Bending Activation. *J. Am. Chem. Soc.* **2013**, *135* (22), 8189-8192. DOI: 10.1021/ja403757p.

(12) Diesendruck, C. E.; Steinberg, B. D.; Sugai, N.; Silberstein, M. N.; Sottos, N. R.; White, S. R.; Braun, P. V.; Moore, J. S. Proton-Coupled Mechanochemical Transduction: A Mechanogenerated Acid. *J. Am. Chem. Soc.* **2012**, *134* (30), 12446-12449. DOI: 10.1021/ja305645x.

(13) Gossweiler, G. R.; Hewage, G. B.; Soriano, G.; Wang, Q.; Welshofer, G. W.; Zhao, X.; Craig, S. L. Mechanochemical Activation of Covalent Bonds in Polymers with Full and Repeatable Macroscopic Shape Recovery. *ACS Macro Lett.* **2014**, *3* (3), 216-219. DOI: 10.1021/mz500031q.

(14) Di Giannantonio, M.; Ayer, M. A.; Verde-Sesto, E.; Lattuada, M.; Weder, C.; Fromm, K. M. Triggered Metal Ion Release and Oxidation: Ferrocene as a Mechanophore in Polymers. *Angew. Chem.* **2018**, *57* (35), 11445-11450. DOI: 10.1002/anie.201803524.

(15) Sha, Y.; Zhang, Y.; Xu, E.; Wang, Z.; Zhu, T.; Craig, S. L.; Tang, C. Quantitative and Mechanistic Mechanochemistry in Ferrocene Dissociation. *ACS Macro Lett.* **2018**, *7* (10), 1174-1179. DOI: 10.1021/acsmacrolett.8b00625.

(16) Wang, S.; Hu, Y.; Kouznetsova, T. B.; Sapir, L.; Chen, D.; Herzog-Arbeitman, A.; Johnson, J. A.; Rubinstein, M.; Craig, S. L. Facile Mechanochemical Cycloreversion of Polymer Cross-Linkers Enhances Tear Resistance. *Science* **2023**, *380* (6651), 1248-1252. DOI: 10.1126/science.adg3229.

(17) Wang, Z.; Zheng, X.; Ouchi, T.; Kouznetsova, T. B.; Beech, H. K.; Av-Ron, S.; Matsuda, T.; Bowser, B. H.; Wang, S.; Johnson, J. A.; et al. Toughening Hydrogels through Force-Triggered Chemical Reactions That Lengthen Polymer Strands. *Science* **2021**, *374* (6564), 193-196. DOI: doi:10.1126/science.abg2689.

(18) Shieh, P.; Nguyen, H. V.; Johnson, J. A. Tailored Silyl Ether Monomers Enable Backbone-Degradable Polynorbornene-Based Linear, Bottlebrush and Star Copolymers through Romp. *Nat. Chem.* **2019**, *11* (12), 1124-1132. DOI: 10.1038/s41557-019-0352-4.

(19) Miller, K. A.; Morado, E. G.; Samanta, S. R.; Walker, B. A.; Nelson, A. Z.; Sen, S.; Tran, D. T.; Whitaker, D. J.; Ewoldt, R. H.; Braun, P. V.; et al. Acid-Triggered, Acid-Generating, and Self-Amplifying Degradable Polymers. *J. Am. Chem. Soc.* **2019**, *141* (7), 2838-2842. DOI: 10.1021/jacs.8b07705.

(20) Binauld, S.; Stenzel, M. H. Acid-Degradable Polymers for Drug Delivery: A Decade of Innovation. *Chem. Commun.* **2013**, *49* (21), 2082-2102. DOI: 10.1039/c2cc36589h.

(21) Fu, C.; Xu, J.; Boyer, C. Photoacid-Mediated Ring Opening Polymerization Driven by Visible Light. *Chem. Commun.* **2016**, *52* (44), 7126-7129. DOI: 10.1039/c6cc03084j.

(22) Dicker, M. P. M.; Baker, A. B.; Iredale, R. J.; Naficy, S.; Bond, I. P.; Faul, C. F. J.; Rossiter, J. M.; Spinks, G. M.; Weaver, P. M. Light-Triggered Soft Artificial Muscles: Molecular-Level Amplification of Actuation Control Signals. *Sci Rep* **2017**, *7* (1), 9197. DOI: 10.1038/s41598-017-08777-2.

(23) Fusi, G.; Del Giudice, D.; Skarsetz, O.; Di Stefano, S.; Walther, A. Autonomous Soft Robots Empowered by Chemical Reaction Networks. *Adv. Mater.* **2023**, *35* (7), e2209870. DOI: 10.1002/adma.202209870.

(24) Yang, C.; Su, F.; Xu, Y.; Ma, Y.; Tang, L.; Zhou, N.; Liang, E.; Wang, G.; Tang, J. pH Oscillator-Driven Jellyfish-Like Hydrogel Actuator with Dissipative Synergy between Deformation and Fluorescence Color Change. *ACS Macro Lett.* **2022**, *11* (3), 347-353. DOI: 10.1021/acsmacrolett.2c00002.

(25) Yang, C.; Su, F.; Liang, Y.; Xu, W.; Li, S.; Liang, E.; Wang, G.; Zhou, N.; Wan, Q.; Ma, X. Fabrication of a Biomimetic Hydrogel Actuator with Rhythmic Deformation Driven by a pH Oscillator. *Soft Matter* **2020**, *16* (12), 2928-2932. DOI: 10.1039/c9sm02519g.

(26) Nagamani, C.; Liu, H.; Moore, J. S. Mechanogeneration of Acid from Oxime Sulfonates. *J. Am. Chem. Soc.* **2016**, *138* (8), 2540-2543. DOI: 10.1021/jacs.6b00097.

(27) Lin, Y.; Kouznetsova, T. B.; Craig, S. L. A Latent Mechanoacid for Time-Stamped Mechanochromism and Chemical Signaling in Polymeric Materials. *J. Am. Chem. Soc.* **2020**, *142* (1), 99-103. DOI: 10.1021/jacs.9b12861.

(28) Hu, Y.; Lin, Y.; Craig, S. L. Mechanically Triggered Polymer Deconstruction through Mechanoacid Generation and Catalytic Enol

Ether Hydrolysis. *J. Am. Chem. Soc.* **2024**, *146* (5), 2876-2881. DOI: 10.1021/jacs.3c10153.

(29) Ameduri, B.; Sawada, H. *Fluorinated Polymers : Volume 2: Applications*; Royal Society of Chemistry, 2016. DOI: 10.1039/9781782626718-fp001.

(30) Shimizu, M.; Hiyama, T. Modern Synthetic Methods for Fluorine-Substituted Target Molecules. *Angew. Chem. Int. Ed.* **2005**, *44* (2), 214-231. DOI: 10.1002/anie.200460441.

(31) Kan, X. W.; Zhang, L. J.; Li, Z. Y.; Du, F. S.; Li, Z. C. Fluoride-Triggered Self-Degradation of Poly(2,4-Disubstitued 4-Hydroxybutyric Acid) Derivatives. *Macromol. Rapid Commun.* **2021**, *42* (18), e2100169. DOI: 10.1002/marc.202100169.

(32) Kleiman, M.; Ryu, K. A.; Esser-Kahn, A. P. Determination of Factors Influencing the Wet Etching of Polydimethylsiloxane Using Tetra-N-Butylammonium Fluoride. *Macromol. Chem. Phys.* **2016**, *217* (2), 284-291. DOI: 10.1002/macp.201500225.

(33) Brubaker, K. S.; Kleiman, M.; Hernandez, L.; Bhattacharjee, A.; Esser-Kahn, A. P. Structural Remodeling of Polymeric Material Via Diffusion Controlled Polymerization and Chain Scission. *Chem. Mater.* **2018**, *30* (22), 8126-8133. DOI: 10.1021/acs.chemmater.8b02293.

(34) Tretbar, C.; Castro, J.; Yokoyama, K.; Guan, Z. Fluoride-Catalyzed Siloxane Exchange as a Robust Dynamic Chemistry for High-Performance Vitrimers. *Adv. Mater.* **2023**, *35* (28), e2303280. DOI: 10.1002/adma.202303280.

(35) Shieh, P.; Zhang, W.; Husted, K. E. L.; Kristufek, S. L.; Xiong, B.; Lundberg, D. J.; Lem, J.; Veysset, D.; Sun, Y.; Nelson, K. A.; et al. Cleavable Comonomers Enable Degradable, Recyclable Thermoset Plastics. *Nature* **2020**, *583* (7817), 542-547. DOI: 10.1038/s41586-020-2495-2.

(36) Brown, C. M.; Husted, K. E. L.; Wang, Y.; Kilgallon, L. J.; Shieh, P.; Zafar, H.; Lundberg, D. J.; Johnson, J. A. Thiol-Triggered Deconstruction of Bifunctional Silyl Ether Terpolymers Via an S(N)Ar-Triggered Cascade. *Chem. Sci.* **2023**, *14* (33), 8869-8877. DOI: 10.1039/d3sc02868b.

(37) Bertolini, J., C. Hydrofluoric Acid: A Review of Toxicity. *J. Emerg. Med.* **1992**, *10* (2), 163-168. DOI: 10.1016/0736-4679(92)90211-b.

(38) Shin, C. H.; Yoon, Y.; Park, J. H.; Ma, B.-C. Design of the Safety Standard at Hydrofluoric Acid Handling Facilities for Risk Reduction. *Korean J. Chem. Eng.* **2018**, *35* (5), 1225-1230. DOI: 10.1007/s11814-018-0013-0.

(39) Dopieralski, P.; Ribas-Arino, J.; Marx, D. Force-Transformed Free-Energy Surfaces and Trajectory-Shooting Simulations Reveal the Mechano-Stereochemistry of Cyclopropane Ring-Opening Reactions. *Angew. Chem. Int. Ed.* **2011**, *50* (31), 7105-7108. DOI: 10.1002/anie.201100399.

(40) Dolbier, W. R.; Keaffaber, J. J.; Burkholder, C. R.; Sellers, S. F.; Koroniak, H.; Pradhan, J. The Thermal Conversion of 6,6-Difluorobicyclo[3.1.0]Hex-2-Ene to Fluorobenzene. A Novel Mechanism. *Tetrahedron Letters* **1991**, *32* (32), 3933-3936. DOI: 10.1016/0040-4039(91)80593-U.

(41) Szychowski, J.; Mahdavi, A.; Hodas, J. J. L.; Bagert, J. D.; Ngo, J. T.; Landgraf, P.; Dieterich, D. C.; Schuman, E. M.; Tirrell, D. A. Cleavable Biotin Probes for Labeling of Biomolecules Via Azide−Alkyne Cycloaddition. *J. Am. Chem. Soc.* **2010**, *132* (51), 18351-18360. DOI: 10.1021/ja1083909.

(42) Parrott, M. C.; Luft, J. C.; Byrne, J. D.; Fain, J. H.; Napier, M. E.; DeSimone, J. M. Tunable Bifunctional Silyl Ether Cross-Linkers for the Design of Acid-Sensitive Biomaterials. *J. Am. Chem. Soc.* **2010**, *132* (50), 17928-17932. DOI: 10.1021/ja108568g.

(43) Grubbs, R. H. *Handbook of Metathesis: Catalyst Development*; Wiley, 2003. DOI: 10.1002/9783527619481.

(44) Wang, F.; Luo, T.; Hu, J.; Wang, Y.; Krishnan, H. S.; Jog, P. V.; Ganesh, S. K.; Prakash, G. K.; Olah, G. A. Synthesis of Gem-Difluorinated Cyclopropanes and Cyclopropenes: Trifluoromethyltrimethylsilane as a Difluorocarbene Source. *Angew. Chem. Int. Ed.* **2011**, *50* (31), 7153-7157. DOI: 10.1002/anie.201101691.

(45) Barbee, M. H.; Kouznetsova, T.; Barrett, S. L.; Gossweiler, G. R.; Lin, Y.; Rastogi, S. K.; Brittain, W. J.; Craig, S. L. Substituent Effects and Mechanism in a Mechanochemical Reaction. *J. Am. Chem. Soc.* **2018**, *140* (40), 12746-12750. DOI: 10.1021/jacs.8b09263.

(46) Price, G. J.; Smith, P. F. Ultrasonic Degradation of Polymer Solutions: 2. The Effect of Temperature, Ultrasound Intensity and Dissolved Gases on Polystyrene in Toluene. *Polymer* **1993**, *34* (19), 4111-4117. DOI: 10.1016/0032-3861(93)90675-Z.

(47) Huang, Y. C.; Chen, C. P.; Wu, P. J.; Kuo, S. Y.; Chan, Y. H. Coumarin Dye-Embedded Semiconducting Polymer Dots for Ratiometric Sensing of Fluoride Ions in Aqueous Solution and Bio-Imaging in Cells. *J. Mater. Chem. B* **2014**, *2* (37), 6188-6191. DOI: 10.1039/c4tb01026d.

(48) Shelef, O.; Gnaim, S.; Shabat, D. Self-Immolative Polymers: An Emerging Class of Degradable Materials with Distinct Disassembly Profiles. *J. Am. Chem. Soc.* **2021**, *143* (50), 21177-21188. DOI: 10.1021/jacs.1c11410.

(49) Kim, H.; Brooks, A. D.; DiLauro, A. M.; Phillips, S. T. Poly(Carboxypyrrole)S That Depolymerize from Head to Tail in the Solid State in Response to Specific Applied Signals. *J. Am. Chem. Soc.* **2020**, *142* (20), 9447-9452. DOI: 10.1021/jacs.0c02774.

(50) Diesendruck, C. E.; Peterson, G. I.; Kulik, H. J.; Kaitz, J. A.; Mar, B. D.; May, P. A.; White, S. R.; Martinez, T. J.; Boydston, A. J.; Moore, J. S. Mechanically Triggered Heterolytic Unzipping of a Low-Ceiling-Temperature Polymer. *Nat. Chem.* **2014**, *6* (7), 623-628. DOI: 10.1038/nchem.1938.

(51) Sirianni, Q. E. A.; Liang, X.; Such, G. K.; Gillies, E. R. Polyglyoxylamides with a pH-Mediated Solubility and Depolymerization Switch. *Macromolecules* **2021**, *54* (22), 10547-10556. DOI: 10.1021/acs.macromol.1c01796.

Table of Contents